

Nanoscale

Accepted Manuscript



This is an *Accepted Manuscript*, which has been through the Royal Society of Chemistry peer review process and has been accepted for publication.

Accepted Manuscripts are published online shortly after acceptance, before technical editing, formatting and proof reading. Using this free service, authors can make their results available to the community, in citable form, before we publish the edited article. We will replace this *Accepted Manuscript* with the edited and formatted *Advance Article* as soon as it is available.

You can find more information about *Accepted Manuscripts* in the [Information for Authors](#).

Please note that technical editing may introduce minor changes to the text and/or graphics, which may alter content. The journal's standard [Terms & Conditions](#) and the [Ethical guidelines](#) still apply. In no event shall the Royal Society of Chemistry be held responsible for any errors or omissions in this *Accepted Manuscript* or any consequences arising from the use of any information it contains.

Cite this: DOI: 10.1039/c0xx00000x

www.rsc.org/xxxxxx

ARTICLE TYPE

Growth of Rutile TiO₂ on Convex Surface of Nanocylinder: From Nanoneedles to Nanorods and Their Electrochemical Properties

Junhua Kong,^a Yuefan Wei,^b Chenyang Zhao,^c Meng Yew Toh,^c Wu Aik Yee,^a Dan Zhou,^a Si Lei Phua,^c Yuliang Dong,^c and Xuehong Lu^{c,*}

Received (in XXX, XXX) Xth XXXXXXXXX 20XX, Accepted Xth XXXXXXXXX 20XX

DOI: 10.1039/b000000x

In this work, bundles of rutile TiO₂ nanoneedles/nanorods are hydrothermally grown on carbon nanofibers (CNFs), forming free-standing mats consisting of three dimensional hierarchical nanostructures (TiO₂-on-CNFs). Morphologies and structure of the TiO₂-on-CNFs are studied using field-emission scanning electron microscope (FESEM), transmission electron microscope (TEM), X-ray diffractometer (XRD) and thermogravimetric analyzer (TGA). Their electrochemical properties as electrodes in lithium ion batteries (LIBs) are investigated and correlated to the morphologies and structure. It is shown that the lateral size of the TiO₂ nanoneedles/nanorods ranges from a few nanometers to tens of nanometers, and increases with the hydrothermal temperature. Small interspaces are observed between individual nanoneedles/nanorods, which are due to the diverging arrangement of nanoneedles/nanorods induced by growing on convex surface of nanocylinder. It is found that the growth process can be divided into two stages: initial growth on the CNF surface and further growth upon re-nucleation on the TiO₂ bundles formed in the initial growth stage. In order to achieve good electrochemical performance in LIBs, the size of the TiO₂ nanostructures needs to be small enough to ensure complete alloying and fast charge transport, while the further growth stage has to be avoided to realize direct attachment of TiO₂ nanostructures on the CNFs, facilitating electron transport. The sample obtained after hydrothermal treatment at 130 °C for 2 hrs (TiO₂-130-2) shows the above features and hence exhibits the best cyclability and rate capacity among all samples; the cyclability and rate capacity of TiO₂-130-2 are also superior to those of other rutile TiO₂-based LIB electrodes.

Introduction

Synthesis of nanostructures has been a hot topic for a few decades since nanomaterials could offer unique and valuable properties for various applications. Tremendous efforts have been devoted to construction of nanostructures with tailored sizes and dimensions, from zero-dimensional (0D) nanospheres and nanoparticles,^[1-2] one-dimensional (1D) nanorods, nanofibers and nanowires,^[3] two-dimensional (2D) nanosheets^[4-7] to three-dimensional (3D) nanoflowers, etc.^[8-9] Among these, 1D nanostructures exhibit some unique features, including large aspect ratio, anisotropic electronic, thermal and mechanical properties, tunable orientation morphology (random or aligned) and ease in preparation via electrospinning, hydrothermal or some other methods. For example, numerous 1D nanostructures of transitional metal oxides,^[10-16] silicon,^[17-20] polymers,^[21-23] carbon^[24-25] and their composites^[26-30] have been successfully prepared and intensively studied as electrodes, catalysts, biomaterials, or in other fields.

Recently, the assembly of low-dimensional (0D/1D/2D) nanostructures into 3D hierarchical ones has been attracting intensive attention as indicated by more than 2000 publications in this area since 2012. Typical examples of 3D hierarchical

nanostructures include nanorod arrays on flat substrate,^[31] nanosheets on nanospheres,^[32] nanowires on nanospheres^[33] and spatially arranged networks of nanoparticles, thin films or nanowires.^[34-35] The benefits of such 3D hierarchical nanostructures are threefold. Firstly, they typically have very high porosity and specific surface area, providing abundant reaction sites, large contact area with surrounded medium or plentiful transport channels for charge carriers. Secondly, the base nanostructures are interconnected or linked by supporting nanostructures, forming continuous networks that would in principle reduce interfacial resistances. Moreover, in 3D hierarchical nanostructures, the features of different low-dimensional nanostructures may be synergistically integrated, evoking favorable interactions and rendering the hierarchical nanostructures some new functions. Concerning the formation of 3D hierarchical nanostructures from 1D nanostructures, extensive work has been carried out.^[36] In particular, nanorods of transitional metal oxides, which have rich applications in electrochemical, photoelectrochemical, catalytic and sensing areas, have been grown from 1D nano/microstructures, such as polymer nanofibers and silicon nanowires, by various routes including hydrothermal growth, chemical etching and chemical vapor deposition.^[37-43] The nanorods in such 3D hierarchical

nanostructures, however, typically have diameters of tens of nanometers or above, or the hierarchical nanostructures are in the form of small particles/powder.^[44-45] Moreover, a clear understanding of growth mechanism of 1D nanostructures on convex surface of other 1D nanostructures is still lacking. Such understanding is essential for tailoring many important properties, such as charge insertion and transport properties, of the 3D hierarchical nanostructures. Establishment of such understanding may enable the control of the morphology so that the properties of the 3D hierarchical nanostructures may be optimized. In this work, TiO₂ 1D nanostructures of various sizes, from a few nanometers to tens of nanometers in diameter, were grown on carbon nanofibers (CNFs) by controlling hydrothermal conditions, forming 3D hierarchical nanostructures (TiO₂-on-CNFs). It is aimed at illustrating the morphological evolution during the hydrothermal growth and revealing the growth mechanism. The electrochemical properties of the free-standing mats of TiO₂-on-CNFs with TiO₂ 1D nanostructures of various sizes are also studied as electrodes in lithium ion batteries (LIBs) in order to establish morphology-property relationships and further improve electrochemical performance of rutile TiO₂-based LIB electrodes.

Experimental section

Materials

Polyacrylonitrile (PAN, $M_w = 150000$), titanium (III) chloride (TiCl₃, ~ 10 wt. % in 20~30 wt% hydrochloric acid) and sodium chloride (NaCl) were purchased from Aldrich Chemistry (USA). Dimethylformamide (DMF) was obtained from Tedia Company Inc (USA).

Preparation of carbon nanofibers as convex substrate

CNFs were prepared by carbonization of electrospun PAN nanofibers as reported previously.^[46] Briefly, PAN was dissolved in DMF by stirring at 60 °C to form a PAN/DMF solution at PAN concentration of 8 wt%. The solution was loaded into a syringe that is connected to a pump system. The electrospinning was conducted for 1 hr under the voltage and feeding rate of 15 kV and 0.4 mL/h, respectively. The PAN nanofibrous mat obtained was dried at 60 °C in vacuum for 24 hrs and then carbonized into CNFs under the following condition: ramping from room temperature to 280 °C at a heating rate of 1 °C min⁻¹ and holding at 280 °C for 1 hr in air atmosphere; then further ramping to 700 °C at a heating rate of 5 °C min⁻¹ and holding at 700 °C for 3 hrs in flowing argon environment.

Growth of TiO₂ on carbon nanofibers

TiO₂ nanostructures were grown on the CNFs via hydrothermal route. In a typical process, 5.3 g NaCl was dissolved in 24.2 g deionized water (DI H₂O), mixed with 6.9 g TiCl₃ solution under stirring at room temperature and then transferred into a Teflon-lined stainless steel autoclave. CNFs mat was put into the above solution and treated at a certain temperature for certain duration in the sealed autoclave. Finally all treated samples were washed by deionized (DI) H₂O and dried at 60 °C in vacuum for 24 hrs. Based on the temperature (T, varies from 90 °C to 180 °C) and the duration (t, maximum 24 hrs) for the treatment, the obtained samples are denoted as TiO₂-T-t accordingly.

Characterization

Field-emission scanning electron microscope (FESEM, JEOL 7600F) and transmission electron microscope (TEM, JEOL 2100) were used to examine the morphologies. The size distribution of the samples was measured statistically from the TEM/FESEM images using ImageJ (100-200 points). Thermogravimetric analyzer (TGA, Q500) was used to measure the composition of the samples. X-ray diffractometer (XRD, Bruker D8 Discover GADDS) with Cu K α radiation was used to investigate the structure of the samples.

Measurements of electrochemical properties

Selected TiO₂-T-t samples were used as working electrode directly. Lithium foil with 14 mm in diameter and 0.6 mm in thickness and 1 M LiPF₆ in the mixture of ethylene carbonate and dimethyl carbonate with 1/1 volumetric ratio were used as counter electrode and electrolyte, respectively. All were assembled into CR2032 battery cells using Celgard 2325 film as separator. The assembly was carried out in argon-filled glove box with oxygen and moisture levels of less than 1 ppm. The assembled batteries were connected to a battery test system (4200, MACCOR) for electrochemical properties study. Cyclic voltammetry (CV) and electrochemical impedance spectroscopy (EIS) studies were performed on an electrochemical workstation (PGSTAT302, Autolab). The voltage window and scan rate were 3.0-1.0 V and 0.5 mV s⁻¹, respectively, for the CV tests, while the frequency range and a.c. amplitude were 10⁵-10⁻² Hz and 5 mV, respectively, for EIS studies.

Results and discussion

Morphologies and structures of TiO₂-on-CNFs

Pure CNFs with average diameter of 300 nm were obtained in free-standing mat form after electrospinning and carbonization of PAN (cf. Fig. S1). The CNFs have rough surface due to the release of gaseous byproducts during the carbonization, facilitating the nucleation of TiO₂ on the CNF surface in hydrothermal processes. The hydrothermal growth, referring to the experimental section, was carried out at 90 °C, 110 °C, 130 °C, 160 °C and 180 °C, respectively, for 24 hrs for structural and morphological investigation, and the obtained samples are denoted as TiO₂-90-24, TiO₂-110-24, TiO₂-130-24, TiO₂-160-24 and TiO₂-180-24, respectively. The low-magnification FESEM images, as displayed in Fig. 1a₁-1d₁, show that the CNFs are fully wrapped by bundles of TiO₂ nanostructures after the hydrothermal treatment. The nanofibrous morphology is still distinctive for the mats obtained at 90 °C to 160 °C, in which most TiO₂ bundles are anchored on the CNFs (Fig. 1a₂-1d₂). In the sample treated at 90 °C (TiO₂-90-24), the TiO₂ bundles are tightly touching each other but with distinguishable boundaries in-between (Fig. 1a₂), while in other samples, wider gaps can be observed between the TiO₂ bundles. When treated at 180 °C, in addition to the TiO₂ bundles on the CNF surface, large particles that are linked to the TiO₂ bundles are also formed on the surface of the mat (Fig. 1e₁). This is likely to be caused by the “following-up” heterogeneous nucleation and growth on the TiO₂ bundles at higher temperature.^[47] Despite the variation of the growth temperatures, the diameters of the “wrapped” nanofibers

Cite this: DOI: 10.1039/c0xx00000x

www.rsc.org/xxxxxx

ARTICLE TYPE

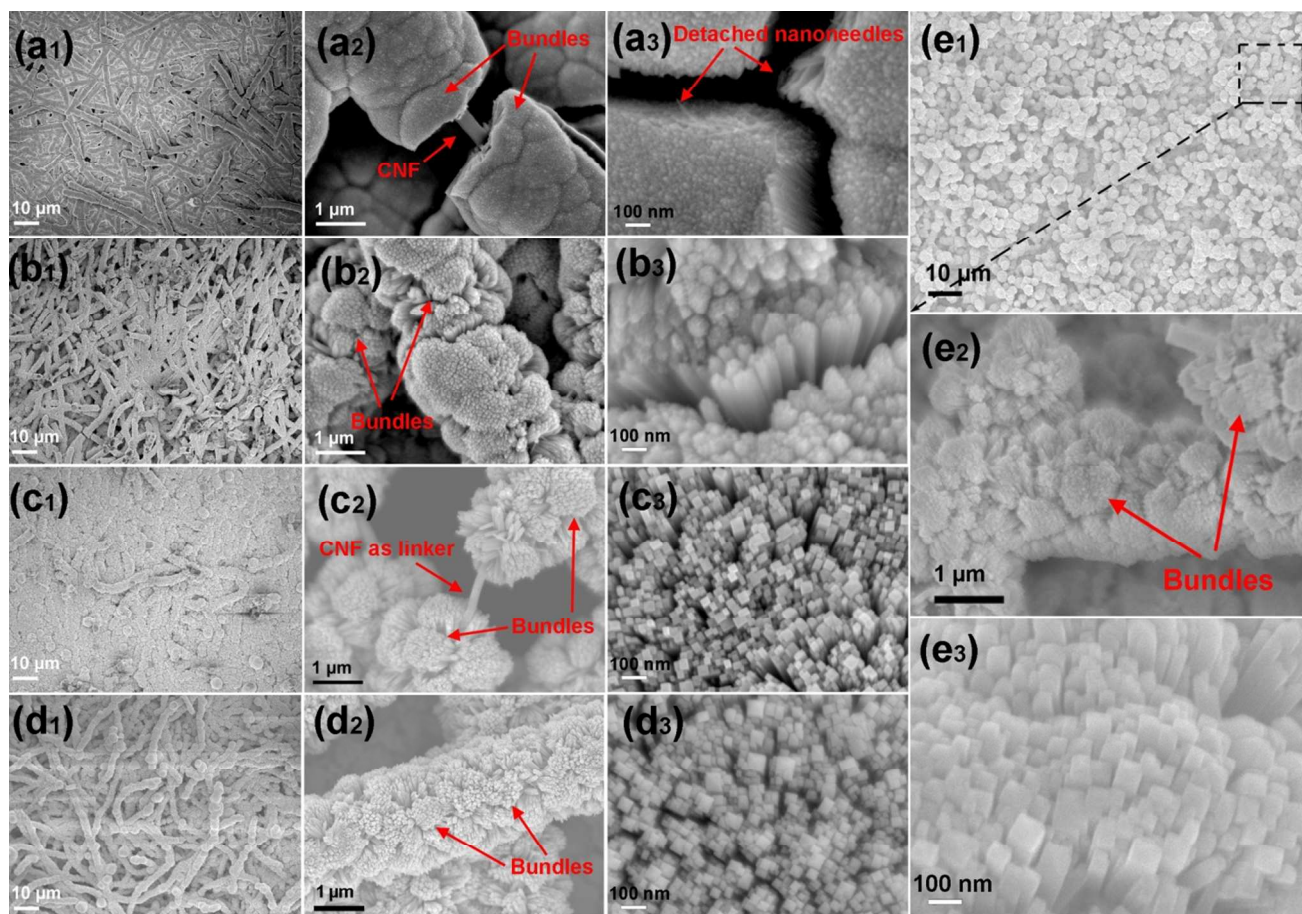


Fig. 1 FESEM images showing TiO_2 nanostructures on carbon nanofibers obtained at hydrothermal temperatures of (a₁-a₃) 90 °C (TiO_2 -90-24), (b₁-b₃) 110 °C (TiO_2 -110-24), (c₁-c₃) 130 °C (TiO_2 -130-24), (d₁-d₃) 160 °C (TiO_2 -160-24) and (e₁-e₃) 180 °C (TiO_2 -180-24). The hydrothermal treatment time was 24 hours for all

5 after hydrothermal treatment of 24 hrs are alike to each other, indicating the similar length of the TiO_2 nanostructures (1-3 μm).

Fig. 2 shows morphologies of the 1D TiO_2 nanostructures in a bundle. For the samples grown at 90 °C (TiO_2 -90-24) and 110 °C (TiO_2 -110-24), the bundles are consisted of TiO_2 nanoneedles, as shown in Fig. 1a₃-1b₃ and Fig. 2a₁-2a₂. The nanoneedles are uniform in diameter, between which small interspaces can be observed (Fig. 2a₂-b₂). Such interspaces offer potential pathways for diffusion of electrolyte and charges, facilitating the redox process during electrochemical application which will be discussed later. The size distributions of the nanoneedles obtained from TEM images (Fig. 3a) show average diameters of about 3.9 nm and 5.2 nm for TiO_2 -90-24 and TiO_2 -110-24, respectively. The data also indicate that the average diameter of the TiO_2 nanoneedles increases with the increase of hydrothermal temperature. The diameters determined from TEM are consistent with the grain sizes calculated from [110] X-ray diffraction peak, *i.e.*, 3.2 nm for TiO_2 -90-24 and 4.8 nm for TiO_2 -110-24 (Fig. 3b), showing the single crystalline nature of each nanoneedle. The

rutile crystal structure of the nanoneedles is verified by both XRD and high-resolution TEM (HRTEM) studies (Fig. 2a₃, 2b₃-2b₄). The growth direction of the TiO_2 nanoneedles is along [110] plane with *d* spacing of 0.32 nm. When the hydrothermal temperatures are 130 °C and higher, the bundles are composed of TiO_2 nanorods of much larger lateral dimension (Fig. 1c₃-1e₃ and Fig. 2c₁-2e₁). Compared with those obtained at lower temperatures, larger interspaces exist between the nanorods grown at 130-180 °C. The statistical size distribution results based on corresponding FESEM images, as displayed in Fig. 3a, indicate broader diameter distribution for the samples obtained at 130 °C (TiO_2 -130-24), 160 °C (TiO_2 -160-24) and 180 °C (TiO_2 -180-24) than those at lower temperatures. The average diameters and diameter ranges of TiO_2 -130-24, TiO_2 -160-24 and TiO_2 -180-24 are 25 nm and 9-55 nm, 33 nm and 14-75 nm, and 60 nm and 28-107 nm, respectively, further confirming the ascending trend of the lateral size with the increase of temperature. The XRD results (Fig. 3b) show that the grain sizes for [110] plane are 9.6, 15.7 and 14.7 nm for TiO_2 -130-24, TiO_2 -160-24 and TiO_2 -180-

Cite this: DOI: 10.1039/c0xx00000x

www.rsc.org/xxxxxx

ARTICLE TYPE

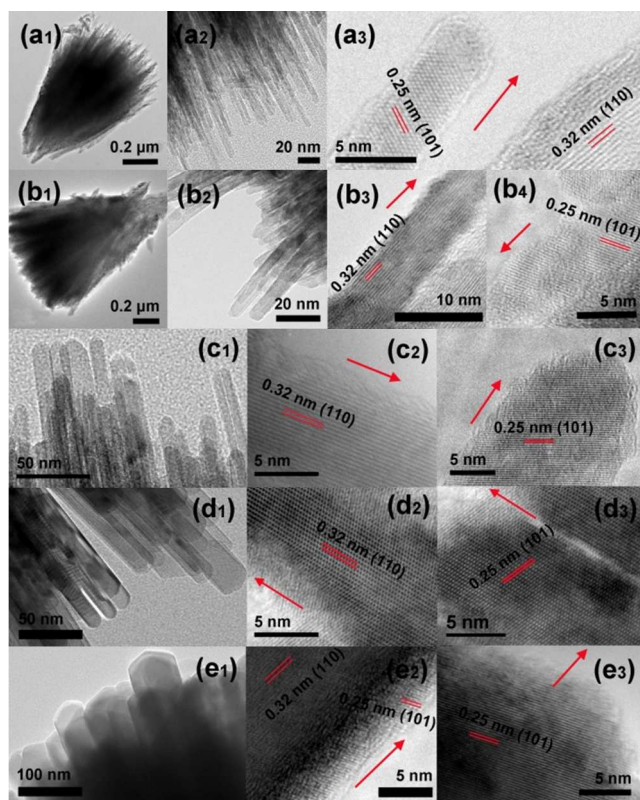


Fig. 2 TEM and HRTEM images of TiO₂ nanostructures on carbon nanofibers obtained at hydrothermal temperatures of (a₁-a₄) 90 °C (TiO₂-90-24), (b₁-b₄) 110 °C (TiO₂-110-24), (c₁-c₃) 130 °C (TiO₂-130-24), (d₁-d₃) 160 °C (TiO₂-160-24) and (e₁-e₃) 180 °C (TiO₂-180-24). The red arrows indicate the length (growth) direction of the TiO₂ nanoneedles/nanorods

24, respectively, which are smaller than the corresponding average diameters of the TiO₂ nanorods. This reveals the polycrystalline nature of the nanorods. It is worth noting that for TiO₂-130-24 and TiO₂-160-24, some small-diameter nanorods may still be single crystalline, whereas all the nanorods in TiO₂-180-24 are of polycrystalline since the grain size is out of the diameter range. Similarly, the growth direction is along [110] plane for the samples as confirmed by HRTEM images (Fig. 2c₂-2c₃, 2d₂-2d₃, 2e₂-2e₃).

The above results show that the dimension and arrangement of the TiO₂ nanostructures on CNFs vary with the hydrothermal temperature when TiCl₃ is used as the precursor. We also found that under the same hydrothermal conditions, different morphologies, for instance, nanorods with much larger lateral size (>100 nm), are produced from other precursors (cf. Fig. S2). This is probably caused by different physical and chemical properties of the precursors that significantly affect the facet structure and dimension of the nuclei formed from the decomposition of the precursors, as well as the growth rates in both diameter and length directions.

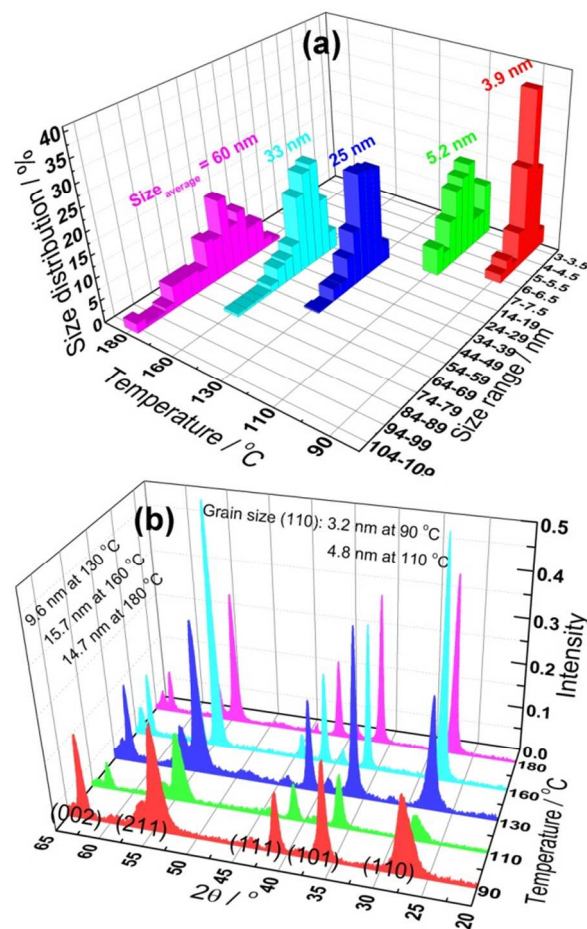


Fig. 3 (a) Size distribution and (b) XRD patterns of the TiO₂ nanoneedles/nanorods on carbon nanofibers obtained at hydrothermal temperatures of 90 °C (TiO₂-90-24), 110 °C (TiO₂-110-24), 130 °C (TiO₂-130-24), 160 °C (TiO₂-160-24) and 180 °C (TiO₂-180-24)

To understand the growth mechanism, further studies were conducted to reveal the detailed growth process of the TiO₂ nanoneedles at low temperatures (< 130 °C). Herein TiO₂-90-24 is used as an example. From the cross-sectional and side views of a broken TiO₂-90-24 sample (Fig. 1a₂, Fig. 4a and 4b), it can be seen that the CNFs are completely wrapped by bundles of TiO₂ nanoneedles, and the bundles touch each other with clear boundaries in between (highlighted by the green dash lines). Visible diverging lines of the bundles can be seen clearly between the green dash lines. Immediately next to the CNFs, some “nuclei” could be observed. The TiO₂ nanoneedles seem to grow from these “nuclei” radially until they touch each other. In order to further clarify the growth mechanism, hydrothermal duration was reduced from 24 hrs to a few hours (t) and the obtained samples are denoted as TiO₂-90-t. It is observed that after growth for 5 h (TiO₂-90-5), the CNFs are nearly bare with only some particles on the surface (Fig. 4c₁). These particles are regarded as “initial nuclei” which then grow into flower-like small bundles

Cite this: DOI: 10.1039/c0xx00000x

www.rsc.org/xxxxxx

ARTICLE TYPE

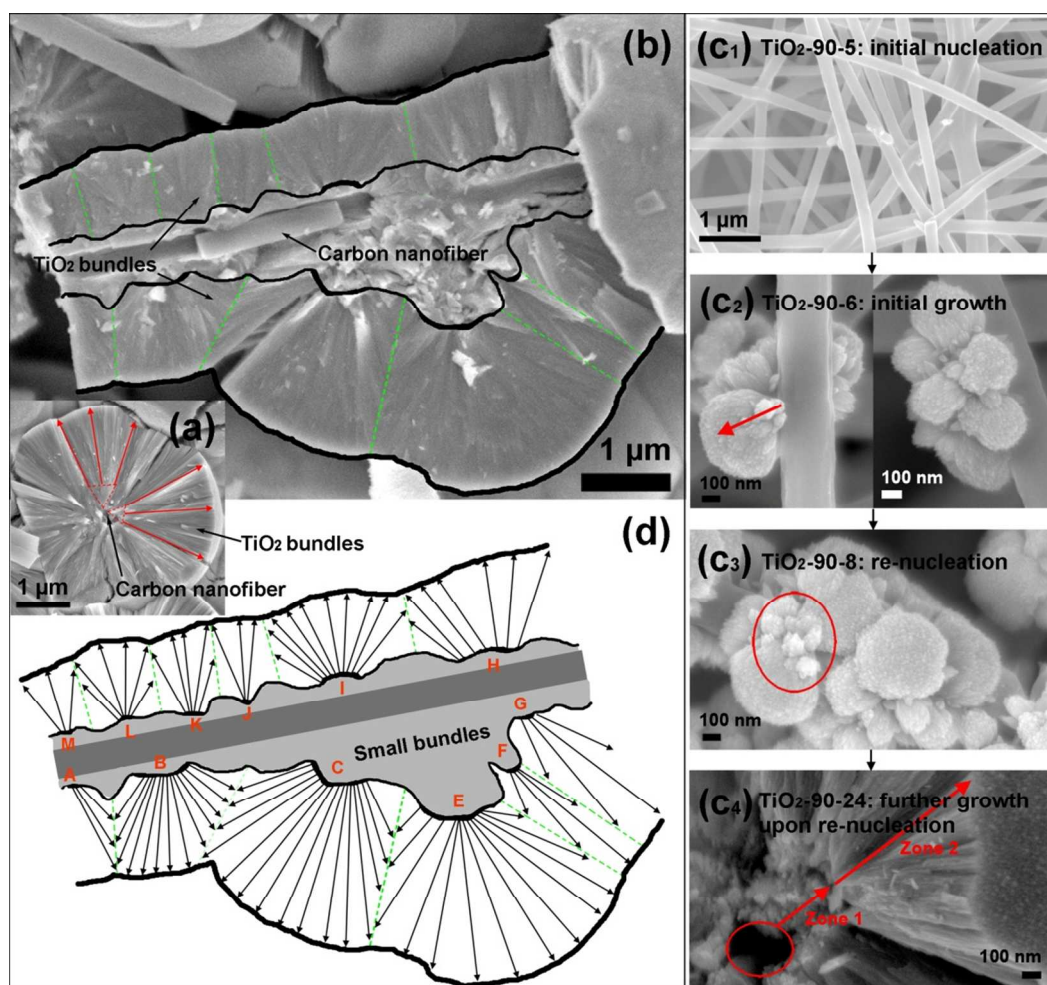


Fig. 4 (a) Cross sectional and (b) side views of a broken TiO₂-90-24 sample. The growth process of TiO₂ nanoneedles at 90 °C from the hydrothermal time of (c₁) 5 hrs (TiO₂-90-5), (c₂) 6 hrs (TiO₂-90-6), (c₃) 8 hrs (TiO₂-90-8) and (c₄) 24 hrs (TiO₂-90-24). (d) A scheme showing the growth of TiO₂ nanoneedle bundles from flower-like “nuclei”

with length of about 500 nm (TiO₂-90-6, Fig. 4c₂). This demonstrates that different from the growth on flat substrate which normally achieves aligned arrays, the use of CNFs offers convex surface as the substrate, leading to initial diverging growth. The jagged gaps between the “flowers” induce re-nucleation (circled area in Fig. 4c₃) for further growth into bundles of TiO₂ nanoneedles of 1-3 μm. The FESEM image in Fig. 4c₄ clearly shows the different morphologies of the TiO₂ nanoneedles from the initial growth (zone 1) and further growth upon the re-nucleation (zone 2). The growth patterns of the TiO₂ nanoneedles observed in Fig. 4b and Fig. 4c are schematically presented in Fig. 4d.

It is believed that at a fixed temperature, the growth rate changes with the time since as the hydrothermal growth proceeds the precursor concentrations decrease. Therefore it is difficult to precisely quantify the growth rates. To demonstrate the influence of temperature on growth rates, the average growth rates in the

initial stage at low and high temperatures were recorded. For the growth at 90 °C, the TiO₂ bundles grew to length of about 500 nm in 6 hrs. By contrast, when the hydrothermal temperature was 180 °C, it took only about 40 min (0.67 hr) for the bundles to achieve the same length (Figure 5d). Obviously, at 90 °C the average growth rate in the initial stage is much slower than that at 180 °C. By reducing the hydrothermal time to less than 2 hrs at 180 °C, similar morphological evolution as that at lower temperatures, i.e., from initial nucleation, initial growth to re-nucleation and further growth, are observed for the growth at 180 °C (Fig. 5).

Electrochemical properties as electrode of lithium ion batteries

The TiO₂-on-CNFs have unique morphological features, which may render them useful properties in various aspects. For instance, they may provide desired spatial arrangement of nano-

Cite this: DOI: 10.1039/c0xx00000x

www.rsc.org/xxxxxx

ARTICLE TYPE

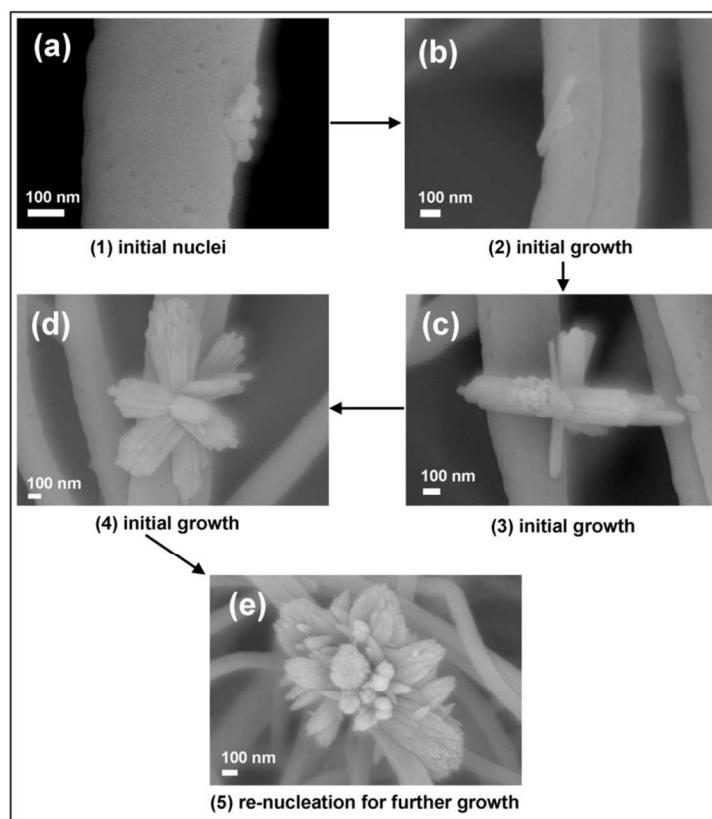


Fig. 5 The growth process of TiO₂ nanorods at 180 °C within hydrothermal time of 2 hrs

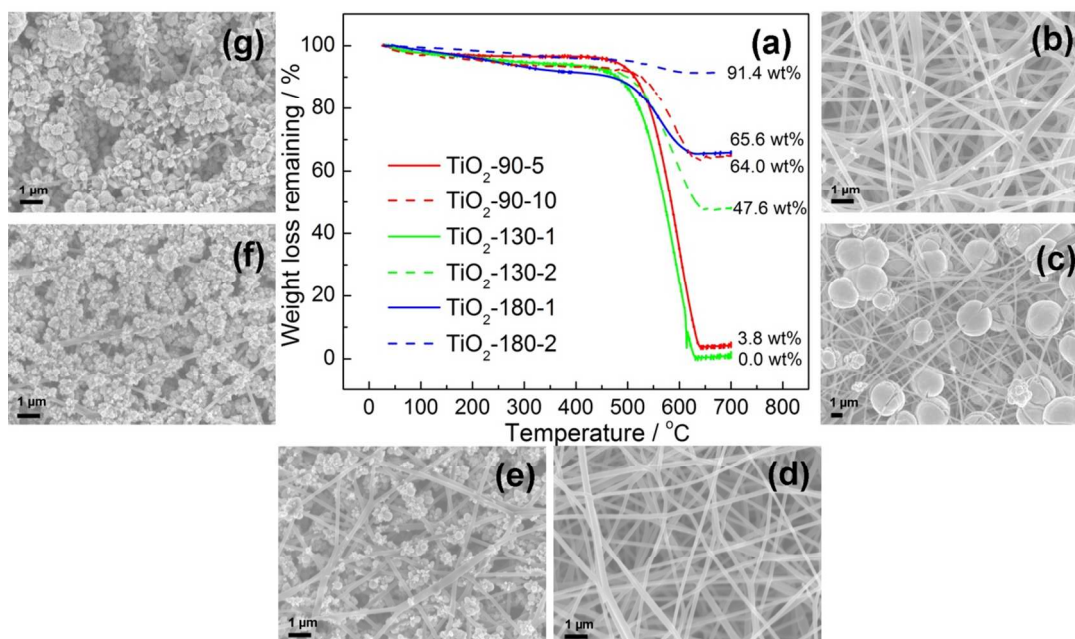


Fig. 6 (a) TGA results of the TiO₂-on-CNFs samples derived at various hydrothermal temperature and time. FEMSEM images of TiO₂-on-CNFs samples derived from (b) 90 °C and 5 hrs (TiO₂-90-5), (c) 90 °C and 10 hrs (TiO₂-90-10), (d) 130 °C and 1 hr (TiO₂-130-1), (e) 130 °C and 2 hrs (TiO₂-130-2), (f) 180 °C and 1 hr (TiO₂-180-1) and (g) 180 °C and 2 hrs (TiO₂-180-2)

Cite this: DOI: 10.1039/c0xx00000x

www.rsc.org/xxxxxx

ARTICLE TYPE

TiO₂ while having TiO₂ content of > 90 wt% (cf. Fig. S3). As for electrochemical applications, different from TiO₂ particles that need binders and conduction agents for charge transport, the as-prepared TiO₂-on-CNFs are in free-standing mat form and therefore can be directly punched into electrode with desired shape and size. The TiO₂ nanoneedles/nanorods are linked by the CNFs that are good electrical conductor, providing conductive path for efficient electron transport during electrochemical reactions. Furthermore, the length and lateral size of the nanoneedles/nanorods can be facily adjusted via controlling the hydrothermal temperature and time, as discussed above.

To demonstrate electrochemical properties of the TiO₂-on-CNFs, the samples obtained at different hydrothermal temperatures were tested as electrodes in LIBs. The cycling and rate capacity is normalized to the mass of TiO₂ since carbon is inactive within the chosen voltage range (1.0-2.8 V, cf. Fig. S4). As an electrode, the composition of the TiO₂-on-CNFs is crucial for achieving good electrochemical performance since TiO₂ is electrochemically active due to its ability of alloying and de-alloying with lithium ions, while carbon is required to be of certain content to provide continuous conduction path for electron transport. For the samples obtained from 24-h hydrothermal growth, the TiO₂ content is higher than 85 wt% (cf. Fig. S3). Such a high TiO₂ content gives unstable cycling capacity (cf. Fig. S5) as majority of the TiO₂ nanoneedles/nanorods are derived in the further growth stage upon re-nucleation, and they are separated from the CNFs by the small TiO₂ flowers grown in the initial stage and hence of indirect contact with the conductor. The charge transport in these nanoneedles/nanorods is inefficient for smooth alloying and de-alloying, leading to severe instability. In order to ensure high electrochemical activity as well as direct contact of most TiO₂ nanoneedles/nanorods with CNFs, the hydrothermal time is

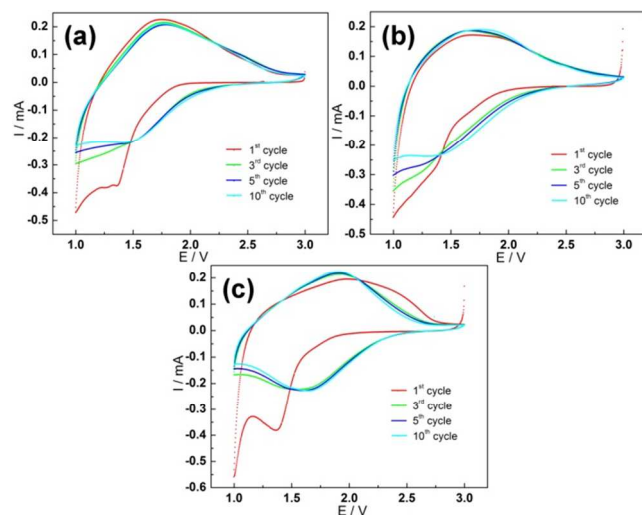


Fig. 7 Cyclic voltammograms of the TiO₂-on-CNFs samples obtained at different hydrothermal temperatures of (a) 90 °C (TiO₂-90-10), (b) 130 °C (TiO₂-130-2) and (c) 180 °C (TiO₂-180-1)

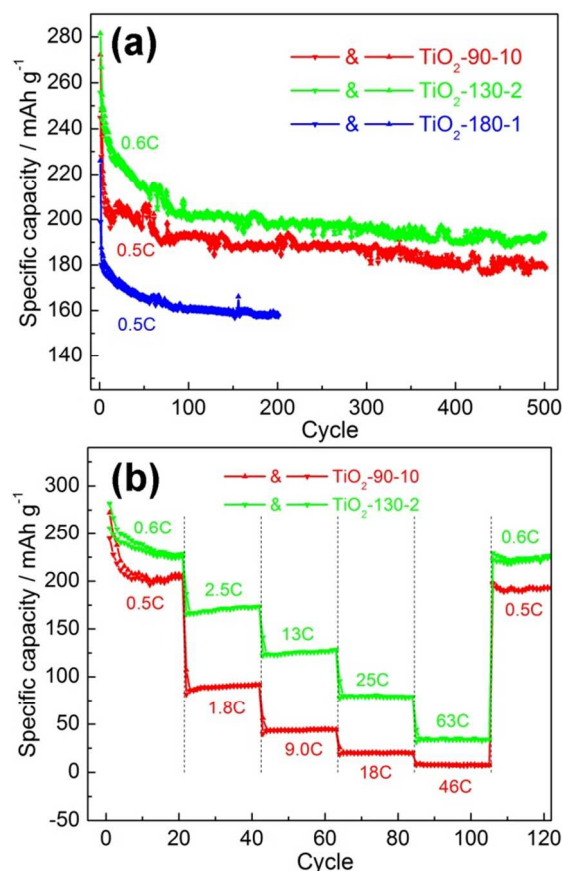


Fig. 8 (a) Cycling capacity and (b) rate capacity of the TiO₂-on-CNFs samples derived from different temperatures of 90 °C, 130 °C and 180 °C

reduced to balance the active content and electrical conduction capability. The content of TiO₂ was determined by TGA (Fig. 6a). By hydrothermal growth at 90 °C for 10 hrs (TiO₂-90-10), 130 °C for 2 hrs (TiO₂-130-2) and 180 °C for 1 hr (TiO₂-180-1), the derived samples possess TiO₂ content of 48-66 wt%. Shorter hydrothermal duration, for instance, 90 °C for 5 hrs (TiO₂-90-5, 3.8 wt%) and 130 °C for 1 hr (TiO₂-130-1, 0 wt%), makes the active content too low, while longer duration, for instance, 180 °C for 2 hrs (TiO₂-180-2, 91.4 wt%), would lead to poor conduction as mentioned earlier. This is verified by the FESEM images displayed in Fig. 6b-6g. For TiO₂-90-10, individual spheres with size of larger than 2 μm are linked by CNFs (Fig. 6c), indicating complete growth of TiO₂ nanoneedles, including initial growth and further growth upon re-nucleation. However, for TiO₂-130-2 and TiO₂-180-1, the length of the bundles on the CNFs is around 500 nm, which is consistent with the length achieved in the initial growth stage, implying that the TiO₂ nanorods in these two samples are mainly formed in the initial growth stage.

The electrochemical properties of TiO₂-90-10, TiO₂-130-2 and TiO₂-180-1, which have reasonable content of active materials, are investigated and compared. Fig. 7 shows the CV of the

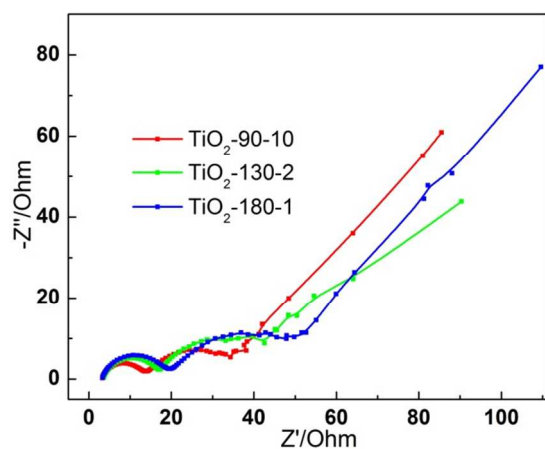


Fig. 9 Nyquist plots obtained from the impedance spectroscopy of TiO₂-on-CNFs derived from different temperatures of 90 °C, 130 °C and 180 °C

5 samples. Typical CV behavior of rutile TiO₂ can be observed which is generally consistent with previous reports.^[44, 48] The peak current intensity decreases in the first few cycles. This is due to the irreversible formation of LiTiO₂ phase from the rutile crystals, which consumes some of TiO₂ and passivates the interfaces. For TiO₂-90-10, TiO₂-130-2, the dominant cathodic peaks appear at about 1.0 V for lithium insertion, while a broad anodic peak appears at around 1.6 V for de-lithiation. For TiO₂-180-1, however, the cathodic and anodic peaks shift significantly to about 1.6 V and 2.0 V, respectively, and the irreversible alloying of TiO₂ with lithium ions at initial cycle (about 1.4 V) occurs much severer than that of TiO₂-90-10, TiO₂-130-2. Such deviation is due to that the grain size of TiO₂ crystals varies under different hydrothermal temperatures.^[48]

The cycling test was conducted at current rate of 50 mA g⁻¹ with respect to the whole electrode, which gives slightly different charging rates for the TiO₂ due to the different compositions (1C is taken as the theoretical capacity of rutile TiO₂, i.e., 168 mA g⁻¹). As for rate capacity measurement, the charging rates also vary for different samples as displayed in Fig. 8. It is shown that the cyclability of all samples becomes more stable after reducing the TiO₂ content. The reversible capacity of TiO₂-130-2 and TiO₂-90-10 are about 200 mAh g⁻¹ and 190 mAh g⁻¹, respectively, which are significantly higher than that of TiO₂-180-1 (Fig. 8a). Under an extremely high charging rate of 25C and 63C, TiO₂-130-2 can still deliver a capacity of 80 mAh g⁻¹ and 35 mAh g⁻¹, respectively, with a remarkable 100 % rebound to around 200 mAh g⁻¹ when the charging rate is reduced back to 0.6C. This is much better than TiO₂-90-10 which possesses lower capacity under even smaller charging rate (Fig. 8b). Therefore the sample derived from hydrothermal growth at 130 °C shows the best electrochemical performance, including low-rate cyclability and rate capacity, which can be attributed to its crystal size, morphology and electron conduction capability. Firstly, small diameter of the nanorods ensures complete alloying of TiO₂ with lithium ions, which is confirmed by the decreased charge transfer resistance with decreasing hydrothermal temperature, i.e., decreasing nanostructure lateral size (Fig. 9). It has also been reported in ref. 49 that nanocrystals with size of 7-12 nm show higher capacity than those with size out of this range. Secondly, the electron transport between the electrode and external circuit

mainly occurs through CNFs during charge/discharge process. The direct contact of TiO₂ with CNFs is necessary for good electrical conduction. For TiO₂-90-10, the growth involves initial growth and further growth upon re-nucleation; the TiO₂ nanoneedles derived from further growth is not in direct contact with CNFs. Thus although TiO₂-90-10 has smaller-diameter nanoneedles and higher TiO₂ content than TiO₂-130-2, some nanoneedles attached in the further growth stage may not be active and hence the performance is poorer than that of TiO₂-130-2.

Conclusion

Bundles of rutile TiO₂ nanoneedles/nanorods were successfully grown on CNFs via hydrothermal route. The diameter of the TiO₂ nanoneedles/nanorods ranges from a few nanometers to tens of nanometers, which can be manipulated by controlling hydrothermal temperature. Distinguishable interspaces are created between individual nanoneedles/nanorods due to the diverging growth on the convex surface. The growth process can be divided into two stages, initial growth of small bundles on the CNF surface and further growth upon the re-nucleation on the small bundles. The electrochemical property studies show that the lateral size of the TiO₂ nanostructures affects charge insertion and transport, while the contact mode (direct or indirect) of the TiO₂ nanoneedles/nanorods with CNFs determines electron conduction capability. These two factors together with the composition of the TiO₂-on-CNFs are important to the electrochemical performance. The TiO₂-on-CNFs obtained by the hydrothermal temperature at 130 °C for 2 hrs exhibits the best cyclability and rate capacity among the three investigated samples. The cyclability and rate capacity of TiO₂-130-2 are also superior to those of other rutile TiO₂-based LIB electrodes.^[44-45, 49] Such TiO₂ nanoneedles/nanorods with tailorable length may also be grown on various curved substrates for other applications, such as for enhancing anti-bacterial functions or solar energy harvest, which would be subjects for future studies.

Notes and references

^a Temasek Laboratories @ NTU, Nanyang Technological University, 9th Storey, BorderX Block, Research Techno Plaza, 50 Nanyang Drive, Singapore 637553

^b School of Mechanical and Aerospace Engineering, Nanyang Technological University, 50 Nanyang Avenue, Singapore 639798

^c School of Materials Science and Engineering, Nanyang Technological University, 50 Nanyang Avenue, Singapore 639798; E-mail: asxhlu@ntu.edu.sg

[†] Electronic Supplementary Information (ESI) available: FESEM image of carbonized electrospinning-derived carbon nanofibers. FESEM images of TiO₂ nanostructures grown on carbon nanofibers using titanium (IV) isopropoxide and titanium (IV) butoxide as precursors. TGA curves of the samples from 24 hrs' hydrothermal growth at 90 °C, 130 °C and 180 °C. The cycling capacity of pure carbon nanofibers at current rate of 50 mA g⁻¹ and voltage range of 1.0-2.8 V. The cycling capacity of the samples from 24 hrs' hydrothermal growth at 90 °C, 130 °C and 180 °C. See DOI: 10.1039/b000000x/

[1] C. Zhu, B. Lu, Q. Su, E. Xie, W. Lan, *Nanoscale* **2012**, *4*, 3060.

[2] S. Mei, Z. Jin, *Small* **2013**, *9*, 322.

[3] Y. Xia, P. Yang, Y. Sun, Y. Wu, B. Mayers, B. Gates, Y. Yin, F. Kim, H. Yan, *Adv. Mater.* **2003**, *15*, 353.

[4] Y. Lin, J. W. Connell, *Nanoscale* **2012**, *4*, 6908.

- [5] P. Innocenzi, L. Malfatti, *Chem. Soc. Rev.* **2013**, *42*, 4198.
- [6] J. H. Liu, X. W. Liu, *Adv. Mater.* **2012**, *24*, 4097.
- [7] T. Govindaraju, M. B. Avinash, *Nanoscale* **2012**, *4*, 6102.
- [8] H. Jiang, P. S. Lee, C. Z. Li, *Energy Environ. Sci.* **2013**, *6*, 41.
- 5 [9] D. C. Meng, M. Erol, A. R. Boccaccini, *Adv. Eng. Mater.* **2010**, *12*, B467.
- [10] T. Krishnamoorthy, V. Thavasi, G. M. Subodh, S. Ramakrishna, *Energy Environ. Sci.* **2011**, *4*, 2807.
- [11] R. Sahay, P. S. Kumar, V. Aravindan, J. Sundaramurthy, W. C. Ling, S. G. Mhaisalkar, S. Ramakrishna, S. Madhavi, *J. Phys. Chem. C* **2012**, *116*, 18087.
- 10 [12] G. Wang, D. Cao, C. Yin, Y. Gao, J. Yin, L. Cheng, *Chem. Mat.* **2009**, *21*, 5112.
- [13] G. Q. Zhang, H. B. Wu, H. E. Hoster, M. B. Chan-Park, X. W. Lou, *Energy Environ. Sci.* **2012**, *5*, 9453.
- 15 [14] Y. F. Wei, L. Ke, J. H. Kong, H. Liu, Z. H. Jiao, X. H. Lu, H. J. Du, X. W. Sun, *Nanotechnol.* **2012**, *23*, 235401.
- [15] Y. Zhou, J.-D. Grunwaldt, F. Krumeich, K. Zheng, G. Chen, J. Stötzler, R. Frahm, G. R. Patzke, *Small* **2010**, *6*, 1173.
- 20 [16] I. Paramasivam, H. Jha, N. Liu, P. Schmuki, *Small* **2012**, *8*, 3073.
- [17] Y. Q. Qu, H. L. Zhou, X. F. Duan, *Nanoscale* **2011**, *3*, 4060.
- [18] K. Q. Peng, S. T. Lee, *Adv. Mater.* **2011**, *23*, 198.
- [19] T. Song, S. T. Lee, B. Q. Sun, *Nano Energy* **2012**, *1*, 654.
- [20] K. Q. Peng, X. Wang, L. Li, Y. Hu, S. T. Lee, *Nano Today* **2013**, *8*, 75.
- 25 [21] S. H. Jiang, H. Q. Hou, A. Greiner, S. Agarwal, *ACS Appl. Mater. Interfaces* **2012**, *4*, 2597.
- [22] L. G. Li, D. L. Jacobs, Y. K. Che, H. L. Huang, B. R. Bunes, X. M. Yang, L. Zang, *Org. Electron.* **2013**, *14*, 1383.
- 30 [23] M. Kurniawan, T. Salim, K. F. Tai, S. Y. Sun, E. J. Sie, X. Y. Wu, E. K. L. Yeow, C. H. A. Huan, Y. M. Lam, T. C. Sum, *J. Phys. Chem. C* **2012**, *116*, 18015.
- [24] M. Inagaki, Y. Yang, F. Y. Kang, *Adv. Mater.* **2012**, *24*, 2547.
- [25] C. Tran, V. Kalra, *J. Power Sources* **2013**, *235*, 289.
- 35 [26] J. Kong, W. A. Yee, Y. Wei, L. Yang, J. M. Ang, S. L. Phua, S. Y. Wong, R. Zhou, Y. Dong, X. Li, X. Lu, *Nanoscale* **2013**, *5*, 2967.
- [27] L. C. Yang, S. N. Wang, J. J. Mao, J. W. Deng, Q. S. Gao, Y. Tang, O. G. Schmidt, *Adv. Mater.* **2013**, *25*, 1180.
- [28] W. Smith, A. Wolcott, R. C. Fitzmorris, J. Z. Zhang, Y. Zhao, *J. Mater. Chem.* **2011**, *21*, 10792.
- 40 [29] Y. Wei, J. Kong, L. Yang, L. Ke, H. R. Tan, H. Liu, Y. Huang, X. W. Sun, X. Lu, H. Du, *J. Mater. Chem. A* **2013**, *1*, 5045.
- [30] J. Kong, Z. Liu, Z. Yang, H. R. Tan, S. Xiong, S. Y. Wong, X. Li, X. Lu, *Nanoscale* **2012**, *4*, 525.
- 45 [31] Y. B. Li, T. Takata, D. Cha, K. Takanabe, T. Minegishi, J. Kubota, K. Domen, *Adv. Mater.* **2013**, *25*, 125.
- [32] D. Han, P. Xu, X. Jing, J. Wang, P. Yang, Q. Shen, J. Liu, D. Song, Z. Gao, M. Zhang, *J. Power Sources* **2013**, *235*, 45.
- [33] G. Bhimarasetti, M. K. Sunkara, *J. Phys. Chem. B* **2005**, *109*, 16219.
- 50 [34] W. Yang, B. Li, *J. Mater. Chem. B* **2013**, *1*, 2525.
- [35] M. Rauber, I. Alber, S. Müller, R. Neumann, O. Picht, C. Roth, A. Schökel, M. E. Toimil-Molares, W. Ensinger, *Nano Lett.* **2011**, *11*, 2304.
- 55 [36] R. K. Joshi, J. J. Schneider, *Chem. Soc. Rev.* **2012**, *41*, 5285.
- [37] J. Kong, Y. Wei, L. Yang, W. A. Yee, Y. Dong, R. Zhou, S. Y. Wong, L. Ke, X. W. Sun, H. Du, X. Li, X. Lu, *J. Phys. Chem. C* **2013**, *117*, 10106.
- [38] I. S. Cho, Z. B. Chen, A. J. Forman, D. R. Kim, P. M. Rao, T. F. Jaramillo, X. L. Zheng, *Nano Lett.* **2011**, *11*, 4978.
- [39] J. Shi, X. Wang, *Energy Environ. Sci.* **2012**, *5*, 7918.
- [40] H. Kim, M. Seol, J. Lee, K. Yong, *J. Phys. Chem. C* **2011**, *115*, 25429.
- [41] Y. Qiu, K. Yan, H. Deng, S. Yang, *Nano Lett.* **2011**, *12*, 407.
- 65 [42] J. Shi, Y. Hara, C. L. Sun, M. A. Anderson, X. D. Wang, *Nano Lett.* **2011**, *11*, 3413.
- [43] B. Yan, S. P. Wang, H. X. Yang, L. J. Feng, H. Y. Wei, Y. Z. Yang, *Asian J. Chem.* **2013**, *25*, 4315.
- [44] J. S. Chen, X. W. Lou, *J. Power Sources* **2010**, *195*, 2905.
- 70 [45] B. Han, S. J. Kim, B. M. Hwang, S. B. Kim, K. W. Park, *J. Power Sources* **2013**, *222*, 225.
- [46] J. Kong, H. R. Tan, S. Y. Tan, F. Li, S. Y. Wong, X. Li, X. Lu, *Chem. Commun.* **2010**, *46*, 8773.
- [47] E. Hosono, S. Fujihara, K. Kakiuchi, H. Imai, *J. Am. Chem. Soc.* **2004**, *126*, 7790.
- 75 [48] N. A. Milne, M. Skyllas-Kazacos, V. Luca, *J. Phys. Chem. C* **2009**, *113*, 12983.
- [49] B. Zhao, R. Cai, S. Jiang, Y. Sha, Z. Shao, *Electrochim. Acta* **2012**, *85*, 636.
- 80